THE JOURNAL OF BIOLOGICAL CHEMISTRY VOL. 286, NO. 41, pp. 35571–35577, October 14, 2011
© 2011 by The American Society for Biochemistry and Molecular Biology, Inc. Printed in the U.S.A.

Role of Amino-terminal Half of the S4-S5 Linker in Type 1 Ryanodine Receptor (RyR1) Channel Gating*

Received for publication, April 27, 2011, and in revised form, August 21, 2011 Published, JBC Papers in Press, August 23, 2011, DOI 10.1074/jbc.M111.255240

Takashi Murayama[‡1], Nagomi Kurebayashi[‡], Toshiharu Oba[§2], Hideto Oyamada[¶], Katsuji Oguchi[¶], Takashi Sakurai[‡], and Yasuo Ogawa[‡]

From the [‡]Department of Cellular and Molecular Pharmacology, Juntendo University Graduate School of Medicine, Tokyo 113-8421, Japan, the [§]Department of Cell Physiology, Nagoya City University Graduate School of Medical Sciences, Nagoya 467-8601, Japan, and the [¶]Department of Pharmacology, School of Medicine, Showa University, Tokyo 142-8555, Japan

The type 1 ryanodine receptor (RyR1) is a Ca^{2+} release channel found in the sarcoplasmic reticulum of skeletal muscle and plays a pivotal role in excitation-contraction coupling. The RyR1 channel is activated by a conformational change of the dihydropyridine receptor upon depolarization of the transverse tubule, or by Ca^{2+} itself, *i.e.* Ca^{2+}-induced Ca^{2+} release (CICR). The molecular events transmitting such signals to the ion gate of the channel are unknown. The S4-S5 linker, a cytosolic loop connecting the S4 and S5 transmembrane segments in six-transmembrane type channels, forms an α-helical structure and mediates signal transmission in a wide variety of channels. To address the role of the S4-S5 linker in RyR1 channel gating, we performed alanine substitution scan of N-terminal half of the putative S4-S5 linker (Thr^{4825}–Ser^{4829}) that exhibits high helix probability. The mutant RyR1 was expressed in HEK cells, and CICR activity was investigated by caffeine-induced Ca^{2+} release, single-channel current recordings, and [^{3}H]ryanodine binding. Four mutants (T4825A, I4826A, S4828A, and S4829A) had reduced CICR activity without changing Ca^{2+} sensitivity, whereas the L4827A mutant formed a constitutive active channel. T4825I, a disease-associated mutation for malignant hyperthermia, exhibited enhanced CICR activity. An α-helical wheel representation of the N-terminal S4-S5 linker provides a rational explanation to the observed activities of the mutants. These results suggest that N-terminal half of the S4-S5 linker may form an α-helical structure and play an important role in RyR1 channel gating.

The type 1 ryanodine receptor (RyR1)[3] is a Ca^{2+} release channel found in the sarcoplasmic reticulum of skeletal muscle and plays an important role in excitation-contraction coupling (1, 2). RyR1 is composed of a homotetramer of an ~565-kDa subunit. A large N-terminal cytoplasmic domain constitutes the "foot" structure that spans the junctional gap between the sarcoplasmic reticulum and transverse tubule, whereas a small C-terminal domain contains the transmembrane segments that form an ion-conducting pore (3). In excitation-contraction coupling, RyR1 is activated by a conformational change of the voltage sensor in the dihydropyridine receptor upon depolarization of the transverse tubule membrane, which is referred to as the depolarization-induced Ca^{2+} release (4, 5). The channel is also activated by Ca^{2+} itself, *i.e.* Ca^{2+}-induced Ca^{2+} release (CICR) (6, 7). The RyR1 channel is regulated by various endogenous ligands, associated proteins, and particular drugs (1, 2). Mapping of ligands and associated proteins onto the RyR1 structure has revealed that most of them are located within the cytoplasmic domain (8). It remains to be elucidated how signals are transmitted from the cytoplasmic domain to the ion gate of the channel upon excitation-contraction coupling or the binding of Ca^{2+} to the channel.

The S4-S5 linker is a cytoplasmic loop connecting the S4 and S5 transmembrane segments in six transmembrane-type channels. In the voltage-gated potassium channels (Kv1.2), the S4-S5 linker forms an α-helical structure and plays an important role in the channel gating (9, 10). The importance of the S4-S5 linker has also been reported in many other channels (11–14). RyR1 is thought to have six or eight transmembrane segments (15), the last two segments may form the outer and inner pore helices with a selective filter between them (16). Substantial similarity in organization of the transmembrane segments between RyR1 and Kv1.2 raises the hypothesis that the S4-S5 linker is involved in RyR1 channel gating (17).

To test the hypothesis, we performed alanine substitution scan of the N-terminal half of the putative S4-S5 linker (Thr^{4825}–Ser^{4829}) that exhibits high helix probability by determining the CICR activity *in vivo* and *in vitro*. The mutant RyR1 channels exhibited an increased or decreased CICR activity by various levels. The impact of each mutant on channel activity can be rationalized by the linker forming an α-helical structure. These findings suggest that the N-terminal half of the S4-S5 linker may form an α-helical structure and play an important role in RyR1 channel gating.

EXPERIMENTAL PROCEDURES

Construction of Expression Plasmids—Cloning and construction of the full-length cDNA cassette encoding the rabbit skel-

* This work was supported in part by grants-in-aid for scientific research from the Japan Society for the Promotion of Science, the Japan Science and Technology Agency (to T. M.), the Vehicle Racing Commemorative Foundation (to N. K.), and the Sportology Center, Juntendo University Graduate School of Medicine (to N. K. and T. S.).

[1] To whom correspondence should be addressed: Dept. of Cellular and Molecular Pharmacology, Juntendo University Graduate School of Medicine, 2-1-1 Hongo, Bunkyo-ku, Tokyo 113-8421, Japan. Tel.: 81-3-5802-1035; Fax: 81-3-5802-0419; E-mail: takashim@juntendo.ac.jp.

[2] Present address: Dept. of Food and Nutritional Sciences, College of Bioscience and Biotechnology, Chubu University, Matsumoto-cho, Kasugai 487-8501, Japan.

[3] The abbreviations used are: RyR, ryanodine receptor; CICR, Ca^{2+}-induced Ca^{2+} release; MH, malignant hyperthermia; AMPPCP, β,γ-methylene adenosine triphosphate.

etal muscle RyR1 (pBS-RyR1) has been described previously (18). The RyR1 cDNA was inserted into pcDNA5/FRT/TO (Invitrogen), a tetracycline-inducible mammalian expression vector. A 0.8-kb 5′-fragment of the cDNA was amplified by PCR using the following primers: 5′-GCAAGCTTCGCCAC-CATGGGTGACGGAGGAGAGGGC-3′ (HindIII site is underlined) and 5′-CAGGTACCGTCCGGTGGTGA-CATG-3′ (KpnI site is underlined) and subcloned into pcDNA5/FRT/TO using the HindIII and KpnI sites. The remaining 14.4-kb 3′-fragment was subcloned into the above plasmid with KpnI and EcoRV sites to generate pcDNA5/FRT/TO-RyR1. Each mutation in the S4-S5 linker corresponding to T4825A, T4825I, I4826A, L4827A, S4828A, and S4829A, was introduced using the QuikChange site-directed mutagenesis kit (Stratagene) with the ClaI (14478)-EcoRV (15248) fragment (pBS-RyR1cs11) as the PCR template (18). The mutations were confirmed by DNA sequencing. The mutated fragment was subcloned into pcDNA5/FRT/TO-RyR1 using the ClaI and EcoRV sites.

Generation of Stable Inducible HEK293 Cell Lines—Flp-In T-REx HEK293 cells (Invitrogen) were maintained in DMEM supplemented with 10% FCS and 2 mM L-glutamine. The stable inducible cell lines were generated by co-transfection of the WT or mutant pcDNA5/FRT/TO-RyR1 vector with the pOG44 vector encoding Flp recombinase according to the manufacturer's instructions. Transfected cells were replated 1 day after transfection, and the growth medium was replaced with selective medium containing 100 μg/ml hygromycin. The selective medium was changed every 3 days until the hygromycin-resistant foci were identified. Several hygromycin-resistant foci were tested for the inducible expression of RyR1, and the selected clones were expanded and stored in liquid nitrogen.

Single-cell Ca^{2+} Imaging—Intracellular Ca^{2+} transients in HEK293 cells expressing WT and mutant RyR1 channels were measured by single-cell Ca^{2+} imaging using fura-2 (23). The cells were plated on the collagen-coated glass-bottomed dishes, and protein expression was induced by doxycycline (1 μg/ml) for 24 h. The cells were loaded with 5 μM fura-2/AM for 30 min at 37 °C in DMEM without FCS and washed with a bath solution (140 mM NaCl, 5 mM KCl, 2 mM $CaCl_2$, 1 mM $MgCl_2$, 11 mM glucose, 5 mM HEPES, pH 7.4). The dish was placed on the stage of an inverted microscope, and fura-2 fluorescence was monitored by a fluorescent monitoring system (Hamamatsu Photonics) with wavelength settings of 340 and 380 nm for excitation (alternating) and 510 nm for emission. Caffeine (0.3–30 mM) was dissolved in the bath solution and perfused into the dishes by suction. Because high concentrations of caffeine affects fura-2 fluorescence intensity to decrease ratio signals (F340/F380) (24), magnitude of Ca^{2+} signals at 10 and 30 mM caffeine were corrected for caffeine effect by multiplying the value by a factor of 1.2 (10 mM caffeine) or 1.6 (30 mM caffeine).

Preparation of Microsomes—Stable HEK293 cells were plated onto ten 100-mm tissue culture dishes and protein expression was induced by doxycycline (1 μg/ml) for 24 h. The cells were harvested, rinsed twice with phosphate-buffered saline, and resuspended in a homogenization buffer (0.3 M sucrose and 20 mM Tris-HCl, pH 7.4, and a protease inhibitor mixture). The cells were disrupted by N_2 cavitation after equilibration in N_2 for 15 min at 1000 psi. The microsomes were obtained by differential centrifugation (1000–100,000 × *g*) and resuspended in the above buffer. The microsomes were quickly frozen using liquid N_2 and stored at −80 °C until use.

Single-channel Recordings—Single-channel recordings were carried out as described previously with CHAPS-solubilized microsomal protein as the material (19, 20). Channel currents were recorded in symmetrical solutions of 250 mM cesium methanesulfonate and 20 mM HEPES/Tris, pH 6.8, at the holding potential of −40 mV (*cis*). Experiments were carried out at 18–22 °C. Bilayers containing only a single channel were used for analysis. Channel currents amplified by an Axopatch 1D patch clamp amplifier (Axon Instruments) were filtered at 1 kHz using an eight-pole low pass Bessel filter and collected at 5 kHz for analysis. The mean open probability (P_o) was calculated from recording durations >2 min by 50% threshold analysis using the pClamp software (version 6.0.4).

[^{3}H]Ryanodine Binding Assay—Ca^{2+}-dependent [^{3}H]ryanodine binding was carried out as described previously (20). Briefly, the microsomes (50–100 μg of protein) were incubated with 8.5 nM [^{3}H]ryanodine for 5 h at 25 °C in a 100-μl solution containing 0.17 M NaCl, 20 mM 3-(*N*-morpholino)-2-hydroxypropanesulfonic acid, pH 6.8, 2 mM dithiothreitol, 1 mM β,γ-methylene adenosine triphosphate (AMPPCP) and various concentrations of free Ca^{2+}. The ionic strength of the solution was kept constant in whole pCa (−log [free Ca^{2+}]) range by using 10 mM Ca-EGTA buffer. The protein-bound [^{3}H]ryanodine was separated by filtering through polyethyleneimine-treated glass filters (Whatman GF/B). Nonspecific binding was determined in the presence of 20 μM unlabeled ryanodine. The [^{3}H]ryanodine binding data (*B*) were normalized to the maximal binding sites for [^{3}H]ryanodine (B_{max}), which was separately determined by Scatchard plot analysis using varied concentrations of [^{3}H]ryanodine (3–40 nM). The B/B_{max} represents an averaged activity of individual channels and can be compared quantitatively between mutants (20, 21). EC_{50} for Ca^{2+} activation and IC_{50} for Ca^{2+} inactivation were calculated by curve-fitting of the Ca^{2+}-dependent [^{3}H]ryanodine binding data as described previously (22).

Data Analysis—Data are presented as the means ± S.E. Statistical comparisons have been made using GraphPad Prism5 software. Student's *t* test was used to compare two groups. *p* values < 0.05 were considered significant.

RESULTS

Expression of Mutant RyR1 Channels with Alanine Substitutions in N-terminal Half of S4-S5 Linker—Fig. 1*A* shows a schematic drawing of the transmembrane topology of the RyR1 channel based on the model according to Du *et al.* (15). The S4-S5 linker is a cytoplasmic loop connecting the S4 and S5 segments. This loop is predicted to be 10 residues in length (Thr^{4825}–Gly^{4834}) (15). The helix probability analysis indicates that its N-terminal half (Thr^{4825}–Ser^{4829}) exhibits high helix probability (Fig. 1*B*) (25). In the voltage-gated potassium channels, formation of an α-helical structure of the S4-S5 linker is critical for channel gating (9, 10). We therefore performed alanine substitution scan of the amino acid residues in the N-terminal half of the putative S4-S5 linker (Thr^{4825}–Ser^{4829}).

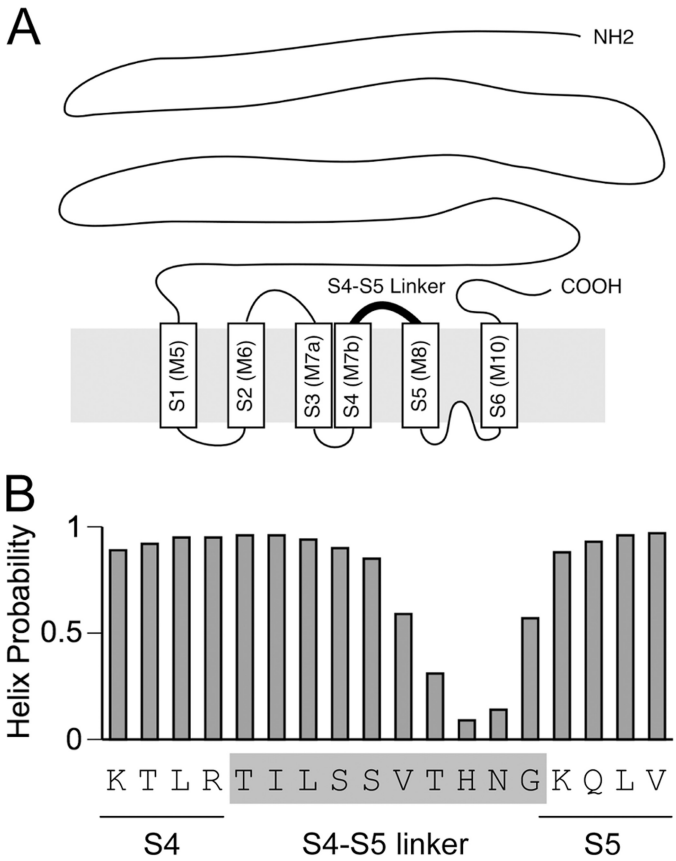

FIGURE 1. **The putative S4-S5 linker in RyR1.** *A*, schematic drawing of the transmembrane topology of the RyR1 channel based on the model according to Du *et al.* (15). The cylinders S1–S6 represent the transmembrane segments that correspond to those originally proposed in the Zorzato model (M5–M10) (34). The putative S4-S5 linker is highlighted by the *boldface line*. *B*, amino acid sequence and the helix probability of the S4-S5 linker in RyR1. The helix probability was predicted by the continuum secondary structure predictor (35, 36). The helix probability is high in the N-terminal half of the S4-S5 linker.

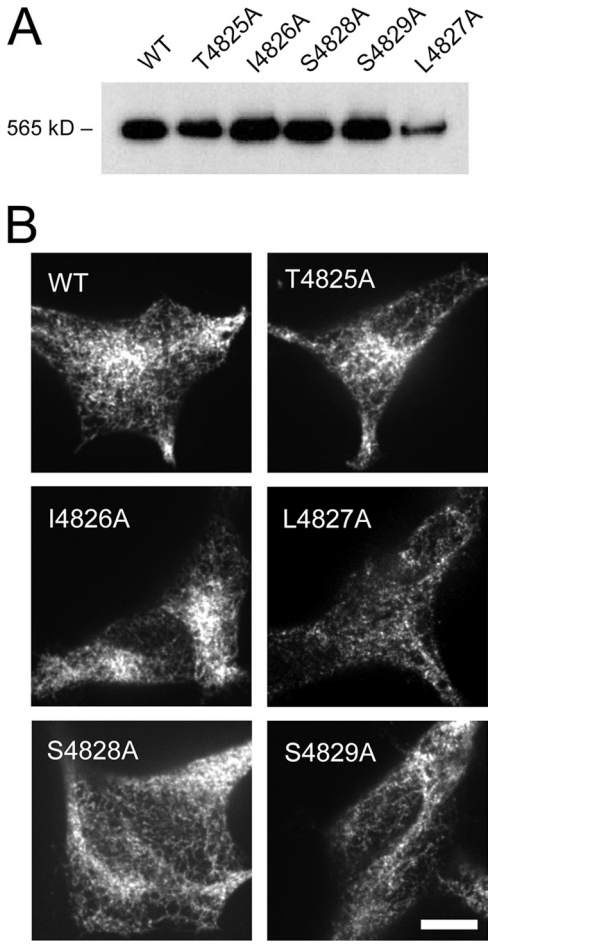

FIGURE 2. **Expression and localization of the mutant RyR1s in HEK cells.** *A*, Western blotting of RyR1 in the lysates from HEK cells expressing WT and the mutant RyR1 carrying alanine substitutions in the S4-S5 linker. The mutant RyR1s showed gel mobility similar to that of the WT. Note that the expression level of L4827A was significantly lower than the other mutants. *B*, immunohistochemical localization of RyR1 in HEK cells. WT and the mutant RyR1s gave rise to similar mesh-like patterns indicative of endoplasmic reticulum localization.

The WT and mutant RyR1 constructs were expressed in HEK cells using a tetracycline-inducible expression system (see "Experimental Procedures"). Fig. 2*A* shows Western blotting of the lysate from these cells. The anti-RyR antibody detected a protein band for a high molecular mass species (565 kDa) in all the cells. No positive bands were observed in mock-transfected cells (data not shown). Besides L4827A, the intensity of the RyR1 band was similar between the mutants, indicating that the levels of protein expression were similar. Fig. 2*B* shows the localization of the mutant RyR1s in HEK cells. As observed for WT, all of the mutants exhibited a mesh-like pattern, indicating endoplasmic reticulum localization of the expressed RyR1. Consistent with the Western blots, the fluorescence intensity of L4827A was lower than that of WT or the other mutants, indicating low levels of expression of this mutant.

Caffeine-induced Ca^{2+} Transients of HEK Cells Expressing Mutant RyR1 Channels—The mutant RyR1 channel was assessed by CICR activity. We initially determined the caffeine-induced Ca^{2+} transients in HEK cells (Fig. 3). Caffeine is a potent activator of CICR and caffeine-induced Ca^{2+} transients well reflect the CICR activity *in vivo* (18). No or only small Ca^{2+} transients were observed with mock-transfected cells with caffeine, indicating negligible level of endogenous RyRs (Fig. 3*A*). Cells expressing WT exhibited caffeine-induced Ca^{2+} transients in a dose-dependent manner: the Ca^{2+} transients increased as the caffeine concentration increased. This is consistent with the previous reports with HEK cells expressing RyR1 (18). The observed decrease in the Ca^{2+} transients at caffeine concentrations $\geq$10 mM may be due to the direct effect of caffeine on the fura-2 ratio signals (24). To determine caffeine sensitivity, the peak magnitude of Ca^{2+} transients was plotted against the caffeine concentration after correction for the caffeine effect (Fig. 3*B*).

All of the alanine-substituted mutants except for L4827A exhibited a reduction in the caffeine sensitivity (Fig. 3*A*). For T4825A, no Ca^{2+} release was observed at 1 mM caffeine, and only small responses were observed at 3 mM caffeine. The effect was more profound for S4829A but less obvious for I4826A and S4828A. The rank order of caffeine sensitivity was WT > I4826A $\fallingdotseq$ S4828A > T4825A > S4829A (Fig. 3*B*). The peak magnitude of Ca^{2+} transients (Fig. 3*B*) and the resting Ca^{2+} level (Fig. 3*C*) for these mutants were similar when compared with the WT species.

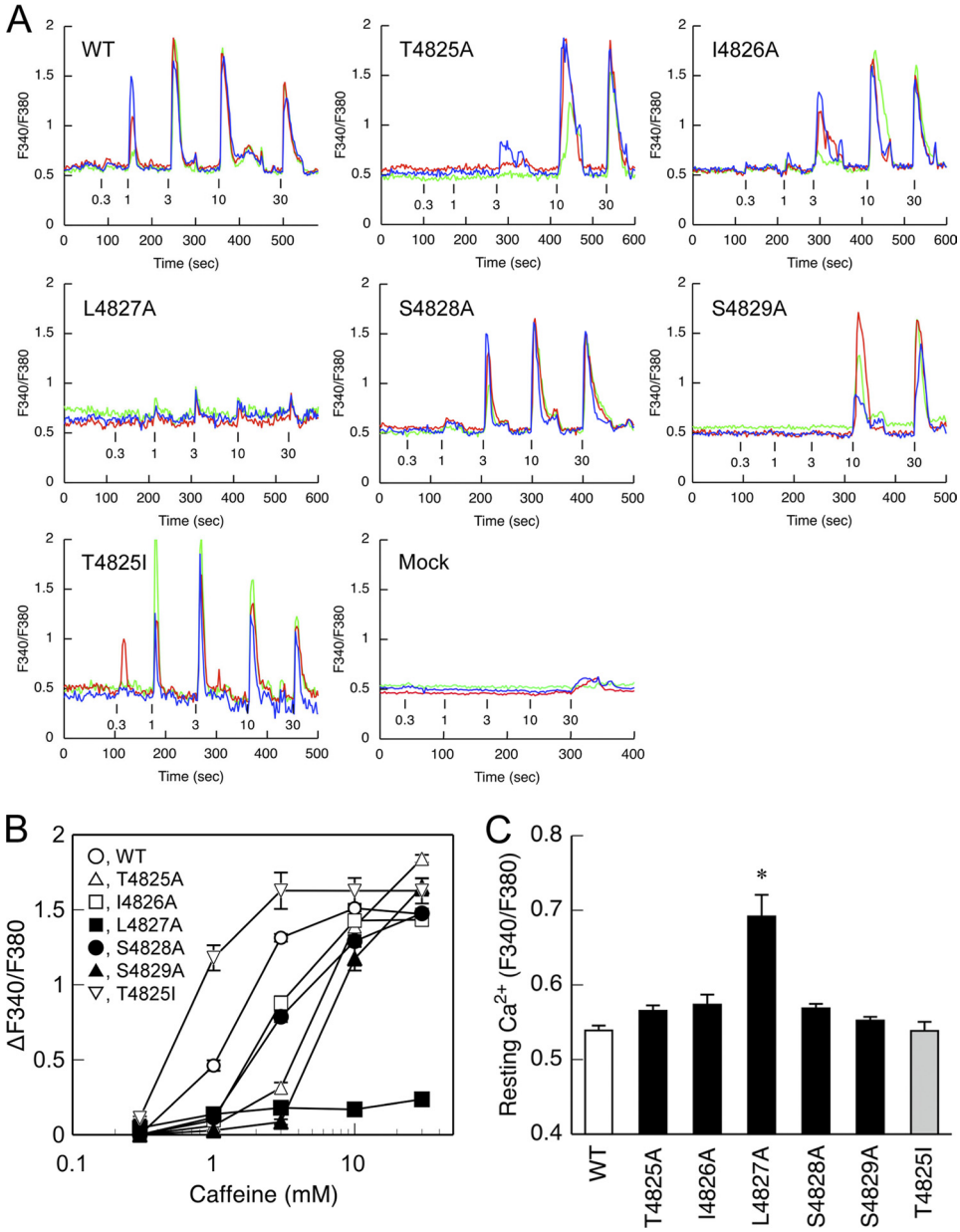

FIGURE 3. **Caffeine-induced Ca^{2+} release in cells expressing WT and mutant RyR1s.** HEK cells expressing WT and the mutant RyR1 channels were loaded with fura-2/AM and stimulated by different concentrations (0.3–30 mM) of caffeine. *A*, three representative traces of fura-2 ratio signals (F_{340}/F_{380}) of single cells for WT and the mutant RyR1s. Caffeine was applied at the time point indicated by the short vertical bars. *B*, the magnitude of Ca^{2+} transients were plotted against caffeine concentrations after correction for the caffeine effect on the fura-2 ratio signals (see "Experimental Procedures"). *C*, resting Ca^{2+} level determined by fura-2 signals (F_{340}/F_{380}) during the first 30 s. L4827A showed significantly greater resting Ca^{2+} than WT and the other mutants. Data are means ± S.E. ($n = 67–100$). *, $p < 0.05$ compared with WT.

L4827A exhibited small but significant Ca^{2+} release at caffeine concentrations ≥1 mM (Fig. 3*A*). The peak magnitude of L4827A was one seventh of that of the WT (Fig. 3*B*). The resting Ca^{2+} level was significantly higher for L4827 than that for WT or the other mutants (Fig. 3*C*). These findings can well be explained by the idea that L4827A constitutes a leaky channel in HEK cells under resting conditions.

Single-channel Current Recordings of Mutant RyR1 Channels—We next recorded the single-channel currents of the mutant RyRs that had been incorporated into planar lipid bilayers. Cs^+ was used for the current carrier instead of Ca^{2+} because conductance for Cs^+ was much greater than that for Ca^{2+} (26). The *cis*-free Ca^{2+} was set at 0.1 mM to optimally activate the channel. The alanine-substituted mutants except for L4827A exhibited lower open probability (P_o) than WT in varied extents (Fig. 4*A*): T4825A and S4829A exhibited a severely reduced P_o when compared with the WT channel, whereas the reduction in P_o was moderate for I4826A and negligible for S4828A. The rank order of mean open probability was WT > S4828A > I4826A > T4825A > S4829A (Fig. 4*B*). No alteration of channel conductance was observed between WT and mutant RyR1 channels (Fig. 4*C*). These findings suggest that these mutant channels have reduced channel opening without alteration of pore formation.

The L4827A channel exhibited a much higher P_o than WT (Fig. 4, *A* and *B*). Possible subconductance states of about one-

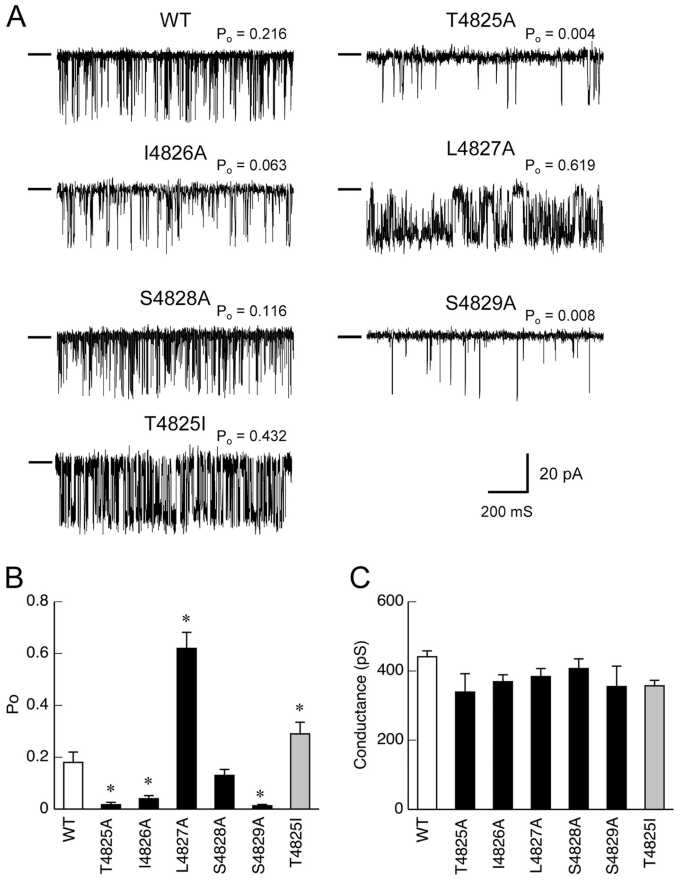

FIGURE 4. **Single Ca^{2+} release channel currents through WT and the mutant RyR1s.** Single-channel currents were recorded at a holding potential of −40 mV (*cis*) in a symmetrical solution containing 250 mM cesium methanesulfonate buffered with 20 mM HEPES/Tris, pH 6.8. Free Ca^{2+} was set at 0.1 mM to optimally activate the channel. *A*, representative traces of single-channel currents through WT and the mutant RyR1 channels. The conductance level of the closed state is shown by a short line on the left side of each current recording. *B*, mean P_o of WT and the mutant channels. *C*, the full open conductance of WT and the mutant channels. Data are means ± S.E. (n = 6–11). *, $p < 0.05$ compared with WT.

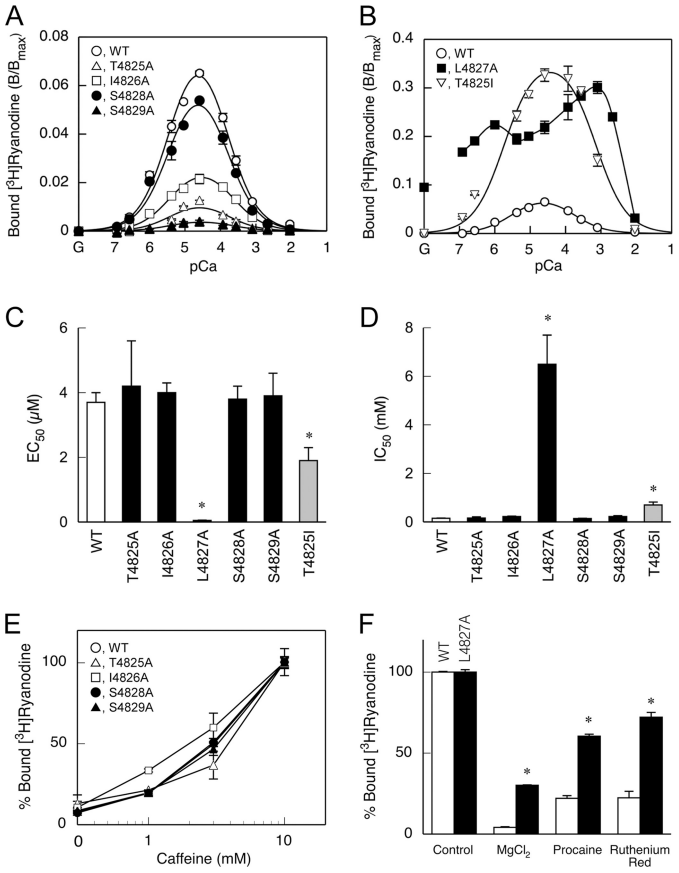

FIGURE 5. **[^{3}H]Ryanodine binding of WT and the mutant RyR1s.** Ca^{2+}-dependent [^{3}H]ryanodine binding was determined in 0.17 M NaCl, 20 mM 3-(*N*-morpholino)-2-hydroxypropanesulfonic acid, pH 6.8, 2 mM dithiothreitol, 1 mM AMPPCP, and various concentrations of Ca^{2+} buffered with 10 mM EGTA. *A* and *B*, Ca^{2+} dependence. Note that the *vertical axis* in B is 5-fold greater than that in *A*. *G* in the *horizontal axis* represents no added Ca^{2+} (10 mM EGTA alone). Four mutants (T4825A, I4826A, S4828A, and S4829A) showed a reduction in [^{3}H]ryanodine binding, whereas the other two mutants (L4827A and the T4825I) showed an increase in [^{3}H]ryanodine binding when compared with the WT protein. *C*, EC_{50} values of Ca^{2+} for activation. *D*, IC_{50} values of Ca^{2+} for inactivation. EC_{50} and IC_{50} values were similar between WT and the four mutants with the reduced activity, whereas the L4827A and T4825I mutants showed smaller EC_{50} and larger IC_{50} values. *E*, effects of caffeine. [^{3}H]Ryanodine binding was determined at pCa 6.7 in the presence of 0–10 mM caffeine. Data were normalized to the values at 10 mM caffeine for each mutant. 100% demotes 0.069, 0.0096, 0.012, 0.053, and 0.0049 B/B_{max} for WT, T4825A, I4826A, S4828A, and S4829A, respectively. *F*, effects of CICR inhibitors. [^{3}H]Ryanodine binding was carried out at pCa 4.5 in the absence and presence of $MgCl_2$ (10 mM), procaine (10 mM), or ruthenium red (10 μM). 100% denotes 0.08 and 0.25 B/B_{max} for WT and L4827A, respectively. L4827A was significantly less sensitive to these inhibitors. Data are means ± S.E. (n = 3–5). *, $p < 0.05$ compared with WT.

fourth and three-fourths of the full conductance level were also seen (Fig. 4*A*). The full open conductance of the mutant channel was not different from that of WT (Fig. 4*C*). Notably, high activity ($P_o = 0.55 \pm 0.09$, $n = 6$) was also observed even at low Ca^{2+} levels (15 mM) (data not shown). Thus, the L4827A mutant constitutes a hyperactive channel.

[^{3}H]Ryanodine Binding of Mutant RyR1 Channels—The CICR activity of the mutant channels was further investigated by [^{3}H]ryanodine binding. Because ryanodine only binds to the open channel, ryanodine binding is widely used as an index of CICR activity (1, 2). The WT RyR1 exhibited biphasic Ca^{2+}-dependent [^{3}H]ryanodine binding with the peak magnitude at 30 μM Ca^{2+} (Fig. 5*A*). The Ca^{2+} concentrations for half-maximal activation (EC_{50}) and inactivation (IC_{50}) for WT were 3.7 ± 0.3 μM and 0.15 ± 0.01 mM, respectively (Fig. 5, *C* and *D*). The biphasic Ca^{2+} dependence is explained by the presence of two distinct Ca^{2+} sites: a high affinity ($K_D \sim$ μM) activating site (A site) and a low affinity ($K_D \sim$ sub-mM) inactivating site (I site). The binding of Ca^{2+} to the A site makes the channel available for activation, whereas the binding of Ca^{2+} to the I site inactivates the channel (22). In addition, magnitude of the Ca^{2+}-dependent activity is determined by another parameter, A_{max}, which represents the gain of the CICR activity (22, 23).

All of the alanine-substituted mutants except for L4827A demonstrated reduced magnitude of ryanodine binding (Fig. 5*A*). The EC_{50} and the IC_{50} values of the mutants for Ca^{2+} were not substantially different from those of WT, indicating no alterations in Ca^{2+} sensitivity (Fig. 5, *C* and *D*). Furthermore, caffeine increased the ryanodine binding to WT and the mutants in a similar dose-dependent manner (Fig. 5*E*). These findings suggest that lower CICR activity of the mutant channels is primarily caused by a reduced gain. The rank order of the peak magnitude was WT > S4828A > I4826A > T4825A > S4829A. This is in accordance with the rank order of caffeine

sensitivity in caffeine-induced Ca^{2+} release (Fig. 3) and of P_o in the single-channel recordings (Fig. 4).

L4827A exhibited high [^{3}H]ryanodine binding in a broad range of Ca^{2+} concentrations (Fig. 5*B*). Substantial [^{3}H]ryanodine binding was observed even in the absence of Ca^{2+} (10 mM EGTA with no added Ca^{2+}). The mutant was less sensitive to inactivating Ca^{2+} (Fig. 5*D*) and CICR inhibitors, including Mg^{2+}, procaine, and ruthenium red (Fig. 5*F*). Consequently, L4827A may represent a constitutively active channel. This well explains that the mutant forms a leaky channel under resting conditions in HEK cells (Fig. 3).

Properties of MH-associated Mutant RyR1 (T4825I)—T4825I is a disease-associated mutation for malignant hyperthermia (27) and is shown to enhance the CICR channel activity (28). To further elucidate the role of the S4-S5 linker, we investigated the T4825I mutant using the above methods under the same conditions. HEK cells expressing T4825I showed higher caffeine sensitivity in caffeine-induced Ca^{2+} release without substantial changes in the peak magnitude and resting Ca^{2+} level (Fig. 3). In single channel recordings, the T4825I channel exhibited a higher P_o than the WT channel (Fig. 4). Possible subconductance states were also seen. Ca^{2+}-dependent [^{3}H]ryanodine binding demonstrated that T4825I had a 5-fold higher peak magnitude than WT with enhanced Ca^{2+} sensitivity for activation and reduced Ca^{2+} sensitivity for inactivation (Fig. 5). Taken together, these results indicate that the T4825I mutation makes the CICR active by both increasing the gain of the channel and altering the Ca^{2+} dependence. This is in marked contrast to the results of the alanine-substituted mutant at the corresponding site (T4825A) showing markedly reduced activity.

DISCUSSION

In this study, we investigated the role of the amino acid residues in the N-terminal half of the putative S4-S5 linker in the RyR1 channel gating using an alanine substitution scan. The CICR activity of the alanine-substituted mutants were determined *in vivo* and *in vitro* by caffeine-induced Ca^{2+} release, single-channel recordings, and [^{3}H]ryanodine binding. We found that four of five mutants (T4825A, I4826A, S4828A, and S4829A) exhibited reduced CICR activity without substantially changing the single-channel conductance and Ca^{2+} or caffeine sensitivity. These findings support the hypothesis that the N-terminal half of the S4-S5 linker may control the gate of the RyR1 channel.

The impact of the alanine substitutions was stronger for the T4825A and S4829A mutations, but lower for the I4826A and S4828A mutations. Fig. 6 demonstrates an α-helical wheel representation of the region from Lys^{4821} to Val^{4830}, which exhibits high helix probability (see Fig. 1*B*). There are two clear faces: polar and basic residues cluster on one face and hydrophobic residues are present on the opposite face. Thr^{4825} and Ser^{4829} are located close to each other and on one face of the helix. Ile^{4826} and Ser^{4828} are not proximal to these two residues. The distribution can explain the varied effects of the alanine substitutions on activity: the face around Thr^{4825} and Ser^{4829} is more important in channel gating than the regions around Ile^{4826} and Ser^{4828}.

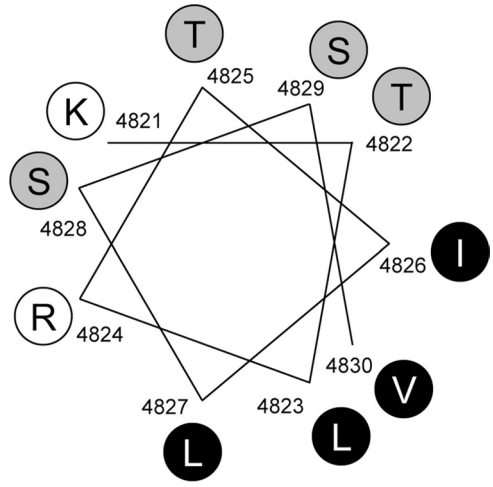

FIGURE 6. **α-Helical projection of the S4-S5 linker region in RyR1.** α-Helical representation of the end of S4 segment and N-terminal half of the S4-S5 linker (Lys^{4821}–Val^{4830}) sequence, which exhibits high helix probability (see Fig. 1*B*). Basic, polar, and hydrophobic residues are depicted in *white*, *gray*, and *black circles*, respectively. Note that there are two clear faces with polar and basic residues on one face and hydrophobic clusters on the opposite face.

The L4827A mutant, in contrast, constituted a leaky channel *in vivo*. The mutant channel exhibited greater P_o than WT with occurrence of possible subconductance states. L4827A had a high activity even in the absence of Ca^{2+} and was much less sensitive to the CICR inhibitors. These findings suggest that L4827A forms a constitutively active channel probably by dysregulation of channel gating. On the α-helical wheel representation, Leu^{4827} is located on the opposite side of Thr^{4825} and Ser^{4829} and forms a hydrophobic cluster with Leu^{4823}, Val^{4830}, and Ile^{4826}. Such a difference might be related to the different effects of the alanine substitutions. I4826A exhibited a slightly reduced CICR activity in contrast to L4827A. This might be explained by location of the residue. The face around Leu^{4827} is more critical in channel gating than the region around Ile^{4826}. Recently, an MH mutation (L4823P) has been reported in Leu^{4823} (29, 30). A detailed investigation of the MH mutant and alanine-substituted mutants for Leu^{4823} and Val^{4830} would provide further support for the role of the hydrophobic cluster.

An MH-associated mutation, T4825I, exhibited enhanced activity when compared with WT, which is consistent with a previous report (28). The phenotype of T4825I was opposite to the alanine-substituted mutant (T4825A), which showed markedly reduced activity. This observation raises the question of why the two mutations had opposite effects on channel activity. Isoleucine has a larger side chain ($-CH(CH_3)CH_2CH_3$) than alanine ($-CH_3$). The side chain of threonine has an intermediate size ($-CH_2(CH_3)OH$). Thus, the size of the side chain at position 4825 might be important in the function of the S4-S5 linker.

How does the S4-S5 linker control the gate in the RyR1 channel? Hamada *et al.* (31) demonstrated that the S4-S5 linker interacts with a 96-kDa fragment of RyR1 containing a calmodulin-like domain (residues 4064–4210). Lee and Allen (25) showed that the S4-S5 linker interacts with the C-terminal tail fragment (residues 4938–5037). It is quite possible that the S4-S5 linker interacts with multiple domains to mediate signal transmission from ligand binding to pore opening.

Because serine and threonine residues can undergo phosphorylation, it is reasonably hypothesized that phosphorylation/dephosphorylation of these residues (Thr^{4825}, Ser^{4828}, and Ser^{4829}) may contribute to channel gating. No consensus sequences, however, are found within the S4-S5 linker for potential phosphorylation sites by protein kinase A, PKC, and CaM kinase II (32). Furthermore, the S4-S5 linker is localized close to the membrane and predicted to interact with the other domains in such restricted space. This might result in a reduced accessibility of kinases/phosphatases. Thus, phosphorylation of these residues seems unlikely.

The amino acid sequence of the putative S4-S5 linker is highly conserved among RyR isoforms: all 10 residues are identical in vertebrate RyR1–3 (1, 2). This suggests that the regulatory mechanism of channel gating via the S4-S5 linker may be shared between the RyR isoforms. Analysis of the RyR2 and RyR3 channels carrying mutations at the corresponding residues would provide further support. High sequence conservation of the S4-S5 linker also raises a possibility of the importance of its C-terminal half. The fact that a disease-associated mutation (H4762P) for catecholaminergic polymorphic ventricular tachycardia has been found within the C-terminal half of the S4-S5 linker in RyR2 may support the possibility (33).

In conclusion, our results strongly support the idea that the N-terminal half of the putative S4-S5 linker plays an important role in the RyR1 channel gating by forming α-helical structure. Further structural and mutational analyses will facilitate our understanding of the interaction and regulatory mechanisms via the S4-S5 linker.

REFERENCES

1. Meissner, G. (1994) *Annu. Rev. Physiol.* **56,** 485–508
2. Ogawa, Y. (1994) *Crit. Rev. Biochem. Mol. Biol.* **29,** 229–274
3. Franzini-Armstrong, C., and Protasi, F. (1997) *Physiol. Rev.* **77,** 699–729
4. Ríos, E., and Pizarro, G. (1991) *Physiol. Rev.* **71,** 849–908
5. Schneider, M. F. (1994) *Annu. Rev. Physiol.* **56,** 463–484
6. Endo, M. (1977) *Physiol. Rev.* **57,** 71–108
7. Endo, M. (2009) *Physiol. Rev.* **89,** 1153–1176
8. Song, D. W., Lee, J. G., Youn, H. S., Eom, S. H., and Kim do, H. (2011) *Prog. Biophys. Mol. Biol.* **105,** 145–161
9. Long, S. B., Campbell, E. B., and Mackinnon, R. (2005) *Science* **309,** 897–903
10. Long, S. B., Campbell, E. B., and Mackinnon, R. (2005) *Science* **309,** 903–908
11. Kuo, A., Domene, C., Johnson, L. N., Doyle, D. A., and Vénien-Bryan, C. (2005) *Structure* **13,** 1463–1472
12. Schug, Z. T., and Joseph, S. K. (2006) *J. Biol. Chem.* **281,** 24431–24440
13. Boukalova, S., Marsakova, L., Teisinger, J., and Vlachova, V. (2010) *J. Biol. Chem.* **285,** 41455–41462
14. Kusch, J., Zimmer, T., Holschuh, J., Biskup, C., Schulz, E., Nache, V., and Benndorf, K. (2010) *Biophys. J.* **99,** 2488–2496
15. Du, G. G., Sandhu, B., Khanna, V. K., Guo, X. H., and MacLennan, D. H. (2002) *Proc. Natl. Acad. Sci. U.S.A.* **99,** 16725–16730
16. Zhao, M., Li, P., Li, X., Zhang, L., Winkfein, R. J., and Chen, S. R. (1999) *J. Biol. Chem.* **274,** 25971–25974
17. Samsó, M., Feng, W., Pessah, I. N., and Allen, P. D. (2009) *PLoS Biol.* **7,** e85
18. Tong, J., Oyamada, H., Demaurex, N., Grinstein, S., McCarthy, T. V., and MacLennan, D. H. (1997) *J. Biol. Chem.* **272,** 26332–26339
19. Oba, T., and Maeno, Y. (2004) *Am. J. Physiol. Cell Physiol.* **286,** C1188-C1194
20. Murayama, T., Oba, T., Hara, H., Wakebe, K., Ikemoto, N., and Ogawa, Y. (2007) *Biochem. J.* **402,** 349–357
21. Murayama, T., Oba, T., Kobayashi, S., Ikemoto, N., and Ogawa, Y. (2005) *Am. J. Physiol. Cell Physiol.* **288,** C1222-C1230
22. Murayama, T., Kurebayashi, N., and Ogawa, Y. (2000) *Biophys. J.* **78,** 1810–1824
23. Murayama, T., and Kurebayashi, N. (2011) *Prog. Biophys. Mol. Biol.* **105,** 134–144
24. Muschol, M., Dasgupta, B. R., and Salzberg, B. M. (1999) *Biophysical journal* **77,** 577–586
25. Lee, E. H., and Allen, P. D. (2007) *Exp. Mol. Med.* **39,** 594–602
26. Fill, M., and Copello, J. A. (2002) *Physiol. Rev.* **82,** 893–922
27. Brown, R. L., Pollock, A. N., Couchman, K. G., Hodges, M., Hutchinson, D. O., Waaka, R., Lynch, P., McCarthy, T. V., and Stowell, K. M. (2000) *Hum Mol. Genet.* **9,** 1515–1524
28. Yang, T., Ta, T. A., Pessah, I. N., and Allen, P. D. (2003) *J. Biol. Chem.* **278,** 25722–25730
29. Sei, Y., Sambuughin, N. N., Davis, E. J., Sachs, D., Cuenca, P. B., Brandom, B. W., Tautz, T., Rosenberg, H., Nelson, T. E., and Muldoon, S. M. (2004) *Anesthesiology* **101,** 824–830
30. Shepherd, S., Ellis, F., Halsall, J., Hopkins, P., and Robinson, R. (2004) *J. Med. Genet.* **41,** e33
31. Hamada, T., Bannister, M. L., and Ikemoto, N. (2007) *Biochemistry* **46,** 4272–4279
32. Kemp, B. E., and Pearson, R. B. (1990) *Trends Biochem. Sci.* **15,** 342–346
33. George, C. H., Jundi, H., Thomas, N. L., Fry, D. L., and Lai, F. A. (2007) *J. Mol. Cell Cardiol.* **42,** 34–50
34. Zorzato, F., Fujii, J., Otsu, K., Phillips, M., Green, N. M., Lai, F. A., Meissner, G., and MacLennan, D. H. (1990) *J. Biol. Chem.* **265,** 2244–2256
35. Bodén, M., and Bailey, T. L. (2006) *Bioinformatics* **22,** 1809–1814
36. Bodén, M., Yuan, Z., and Bailey, T. L. (2006) *BMC Bioinformatics* **7,** 68